Fracture Mechanics of Concrete Structures
Proceedings FRAMCOS-3
AEDIFICATIO Publishers, D-79104 Freiburg, Germany

FRACTURE ENERGY OF STRAIN-HARDENING CEMENTITIOUS COMPOSITES

P. Kabele
Department of Civil Engineering, The University of Tokyo, Tokyo, Japan
V.C. Li
ACE-MRL, Department of Civil and Environmental Engineering, The University of Michigan, Ann Arbor, USA

Abstract
Fracture energy of pseudo strain-hardening cementitious composites is computed by means of finite element analysis of crack growth under small-scale yielding conditions. A parametric study is conducted, which clarifies the relation between the composites' uniaxial behavior and their fracture energy.
Key words: short fiber composites, pseudo strain-hardening, R-curve, small-scale yielding, FEM analysis

1 Introduction

The possibility to control their overall mechanical properties by adjusting micromechanical parameters of their constituents is one of the most important features of composite materials. In this paper, we consider a class of composites consisting of a cementitious matrix and relatively low volume fraction (<2%) of short randomly distributed and randomly oriented fibers. Using an analytical model that relates the composites' post-cracking behavior to their microstructure, it has become possible to *design* composites that under uniform tension undergo extensive multiple cracking and have a significant overall hardening response (Fig. 1), (Li, 1997).

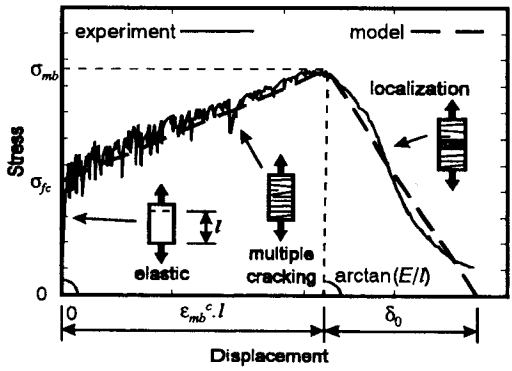

Fig. 1 Typical uniaxial tensile behavior for a pseudo strain-hardening composite

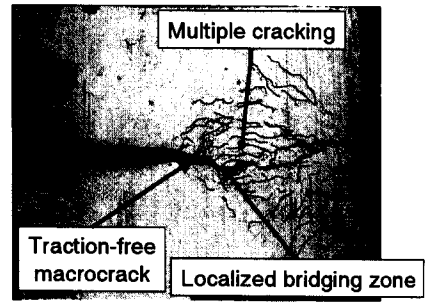

Fig. 2 Cracking of a pseudo strain-hardening composite in front of a notch (photo ACE-MRL)

In the multiple cracking state, the composite exhibits almost uniform distribution of sub-parallel matrix cracks with small crack spacing (several millimeters) and sub-millimeter crack widths (< 0.1 mm). From a macroscopic point of view, the deformation due to these cracks can be seen as an inelastic strain, and the behavior is termed pseudo strain-hardening.

Multiple cracking is possible due to fibers transmitting increasing traction across the matrix cracks as the cracks open. The overall hardening behavior eventually ends when fibers on one of the crack planes cannot carry further increasing load and start to exhibit softening. Consequently, fracture localizes into a single plane.

Furthermore, experiments by Li and Hashida (1992) have shown remarkable behavior of these materials in the presence of a stress concentrator, such as a notch. Propagation of a traction-free crack from the notch tip is accompanied by multiple cracking distributed over a large volume, as well as extension of a bridging zone localized in the main crack plane (see Fig. 2). Such a behavior leads to energy dissipation both off and on the main fracture plane, which results in a significant increase in the composite resistance to the macroscopic crack propagation. This property opens a vast field of applications for these materials, ranging from strain-intensive structural details to penetration-proof structures.

Therefore, a necessity arises to design these composites for target performance given not only in terms of their response to uniaxial tension, but also in terms of crack growth resistance. To be able to fulfill this task, a link is needed that relates the behavior of the composites under uniform uniaxial tension –a property that can be predicted using existing models – to the fracture resistance. The objective of this paper is to clarify the above relationship.

2 Characterization of crack growth resistance in pseudo strain-hardening cementitious composites

2.1 Fracture energy and R-curve

The subject of the present study is a growth of a traction-free macroscopic crack (macrocrack) in a pseudo strain-hardening composite. Crack driving force in a nonlinear material can be expressed in terms of path-independent J integral (Broek, 1991), defined by Rice (1968) as:

$$J = \int_{\Gamma} \left(W dy - \mathbf{t} \frac{\partial \mathbf{u}}{\partial x} ds \right) \tag{1}$$

Here Γ is a contour connecting the macrocrack surfaces and completely surrounding the nonlinear zone at the macrocrack tip, W is the strain-energy density, $\mathbf{t}$ is the traction vector, $\mathbf{u}$ is the displacement vector, and ds is an element of arc length along Γ. The condition for the macrocrack growth is then

$$J = J_c, \tag{2}$$

where J_c is the macrocrack growth resistance. Using Eqn. 2, the resistance can be estimated as the value of the J integral, calculated at the instant when crack extension occurs.

As shown by Rice (1968), under self-similar crack growth conditions, the J integral can be interpreted as a change in potential energy for a virtual crack extension. Thus, resistance J_c can be understood as energy that has to be supplied to create a unit area of the traction-free macrocrack. We call J_c a composite fracture energy.

The supplied energy is consumed in two inelastic processes around the macrocrack tip:

- distributed multiple cracking, where the dissipative mechanism is formation of new matrix cracks and fiber-matrix interface debonding of fibers bridging these cracks;
- degradation of the fiber bridging in the localized process zone, where energy is released mainly through fiber pullout.

Accordingly, Li and Hashida (1992) suggested that the composite fracture energy J_c could be decomposed into two components: off-crack-plane

fracture energy J_m and bridging fracture energy J_b. The first component corresponds to the energy released through multiple cracking, while the latter one to the energy dissipated in the localized bridging zone on the main fracture plane. Bridging fracture energy J_b can be evaluated as J integral taken on a contour enclosing only the localized bridging zone. The off-crack-plane fracture energy J_m is then the difference between J_c and J_b.

During the traction-free macrocrack growth, the extent of the near-tip nonlinear process zone changes. Consequently, the macrocrack growth resistance is not constant, but varies with the amount of crack extension. This behavior is characterized by the R-curve; a plot of the fracture energy (or resistance) J_c against the crack extension length Δa.

2.2 Characterization under small-scale yielding conditions

Under small-scale yielding conditions, it is assumed that the nonlinear zone at the macrocrack tip is very small compared to the crack length and that it is embedded in a stress field, which is dominated by the singularity of elastic solution (Hutchinson, 1968). Considering mode I crack, the singular stress field, also called the K-field, is given in the form of:

$$\sigma_{ij} = \frac{K}{\sqrt{2\pi r}} f_{ij}(\theta), \tag{3}$$

where r and θ are polar coordinates with origin at the traction-free crack tip, $f_{ij}(\theta)$ is a function of angular coordinate θ only (see e.g. Broek, 1991), and K is the mode I stress intensity factor. Under these circumstances, the J integral, taken on a contour connecting the macrocrack surfaces and passing outside of the near-tip nonlinear zone, coincides with the energy release rate G. Furthermore, the G is related to the stress intensity factor K:

$$G = \frac{K^2}{E'}, \tag{4}$$

where E' is the Young's modulus E for plane stress and $E' = E/(1-\nu^2)$ for plane strain, and ν is the Poisson's ratio.

Consequently, the crack growth criterion given by Eqn. 2 can be restated as:

$$G = G_c \quad \text{or} \quad K = K_c \tag{5), (6}$$

where G_c is a composite critical energy release rate. K_c is a composite fracture toughness. Note that, under small-scale yielding conditions, the composite fracture energy J_c and the composite critical energy release rate G_c are identical. In analogy to J_c, G_c can be also decomposed into two components G_m and G_b, which correspond to the energy release rate in the multiple cracking zone and to that on the main crack plane, respectively.

3 Material model

A constitutive model, which captures the cracking behavior of pseudo strain-hardening composites under uniaxial tension (see Section 1) and extrapolates it into a two-dimensional plane stress/plane strain state, has been proposed by Kabele and Horii (1997). We employ this model in the present study. The material in the hardening, multiple cracking state is represented using incremental theory of plasticity, with the Rankine yield function:

$$F \equiv \left(\sigma^*_{xx}+\sigma^*_{yy}\right)/2+\sqrt{\left(\sigma^*_{xx}-\sigma^*_{yy}\right)^2/4+\left(\sigma^*_{xy}+\sigma^*_{yx}\right)^2/4}-\sigma_{fc}=0; \qquad (7)$$

and a linear kinematic hardening rule:

$$\sigma^*_{ij}=\sigma_{ij}-\alpha_{ij} \quad \text{and} \quad d\alpha_{ij}=h d\varepsilon^c_{ij} \qquad (8), (9)$$

Here ε_{ij}^c is an inelastic cracking strain, associated with the width and spacing of the multiple cracks. The parameter h is the slope of a uniaxial stress vs. cracking strain curve and is assumed constant. The parameter σ_{fc} is a first crack strength under uniaxial tension.

It is assumed that a change into a softening regime, and consequently fracture localization, occurs when the maximum principal value of the accumulated cracking strain attains critical level $\varepsilon_{mb}{}^c$. As shown in Fig. 1, this critical value corresponds to the inelastic strain at peak stress σ_{mb} of the uniaxial test. Upon satisfaction of the localization criterion in any element, a discrete discontinuity is embedded into this element in a direction normal to that of the maximum principal cracking strain. The discontinuity surfaces are not immediately traction free, but the normal traction t_n decreases with increasing normal displacement jump across the discontinuity δ_n. The slope of this relationship (tension-softening relationship approximated as linear) is denoted as s. While tensile bridging traction exists, the

discontinuity corresponds to the localized bridging zone, discussed in Section 1. Once the normal traction reaches zero value at $\delta_n=\delta_0$, the discontinuity becomes a traction-free macrocrack.

To summarize, the material model is defined by the following set of parameters:

- Young's modulus E and Poisson's ratio ν in the elastic regime;
- first crack strength σ_{fc}, tensile strength σ_{mb}, critical cracking strain ε_{mb}^{c} and hardening slope $h=\left(\sigma_{mb}-\sigma_{fc}\right)/\varepsilon_{mb}^{c}$ in the hardening multiple cracking regime;
- tensile strength σ_{mb}, critical crack opening displacement δ_0, and tension-softening slope $s=\sigma_{mb}/\delta_0$ in the softening localized cracking regime.

The meaning of each parameter is clear from Fig. 1. Note that, excluding E and ν, only four of the parameters are independent.

It should be also noted that due to employing the tension-softening relationship in the present model, no stress singularity occurs at either the localized bridging zone tip or the traction-free macrocrack tip.

4 Analysis of composite fracture energy under small-scale yielding conditions

Kabele (1995) carried out FE simulations of crack growth under large scale yielding conditions in double cantilever beam specimens made of pseudo strain-hardening composites. The analyses revealed that the specimen boundaries limited free expansion of the off-crack-plane nonlinear zone around the notch tip. As a large portion of total fracture energy J_c (its component J_m) resulted from this nonlinear process, a strong dependence of J_c on a specimen size was observed.

The aim of the present study is to find the resistance curve as a material characteristic, that is, independent of the specimen size. Therefore, we obtain the R-curves from analyses of mode I crack growth under small-scale yielding conditions, which are achieved by embedding the damage and crack bridging zones in a remote K-field.

4.1 Computation of R-curve: model and solution procedure

The analyses are carried out assuming infinitesimal strains and displacements and plane stress state.

The assumptions of small-scale yielding stated in Section 2.2 are realized in the following way. Taking into account symmetry of the problem, a

semi-circular domain with diameter D is considered. The domain is intersected by a notch with length $D/2$, as shown in Fig. 3. Diameter D is 1000 m, which is at least 500-times larger than the height of the largest nonlinear zone in any of the analyzed problems. Traction-free boundary conditions are applied at the notch surface and displacement in y-direction is fixed on the remaining portion of the symmetry axis. Tractions **F**, corresponding to the singular elastic stress field (Eqn. 3) with coordinate r measured from the traction-free macrocrack tip, are applied on the outer semicircular boundary of the domain.

From Eqn. 3 it is clear that load **F** is a function of intensity K of the applied field. When the traction-free macrocrack propagates, **F** also depends on the total crack elongation Δa, as the K-field is to be applied around the traction-free crack tip. Thus:

$$\mathbf{F} = \mathbf{F}(K, \Delta a) \tag{10}$$

The R-curve is then traced using the following incremental procedure:

1. Initially, the traction-free macrocrack tip coincides with the notch tip, thus Δa=0. Load **F** is incrementally changed by increasing the intensity K from zero, while Δa is kept constant. This results in multiple cracking around the notch tip, modeled as continuum hardening plasticity. Further increase of K leads to formation of a localized bridging zone, where tension-softening takes place. This is realized by automatically changing the continuous elements into elements with embedded discontinuity. K is increased until the crack opening displacement in the center of the most strained element just ahead of the notch reaches the critical value of δ_0, at which all the bridging traction is released. This corresponds to a growth of the traction-free crack by the length of a single element, da. From Eqn. 6 it is obvious that at this instant, the crack driving force K is equal to the resistance $K_c(\Delta a=0)$. Thus, we obtained a point of the R-curve.
2. As the traction-free macrocrack extension Δa is now equal to da, the applied load $\mathbf{F}(K=K_c(0),\Delta a=0)$ has to be updated to reflect the new state. This is done by keeping K constant and adding an increment of **F** such, that the total applied load becomes $\mathbf{F}(K=K_c(0),\Delta a=da)$. It is assumed that during this increment no further traction-free crack growth takes place beyond the element that has become critical in step 1.
3. The steps 1. and 2. are repeated with the only difference that variable Δa is initially assigned value Δa(previous step)+da and K is incrementally changed not from zero, but from K_c(previous step).

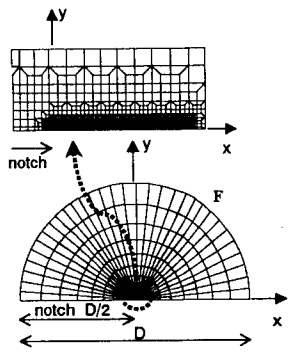

Fig. 3 Finite element mesh used for R-curve computation

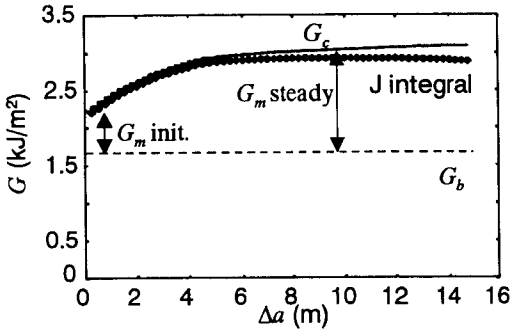

Fig. 4 Computed R-curve

The procedure described above allows tracing the R-curve up to quite a large macrocrack extension, as the origin of the applied K-field is always kept at the actual traction-free crack tip. It should be also noted that, due to the assumption of no further macrocrack growth in step 2., the procedure is applicable only until the resistance increases or is invariant with increasing Δa.

4.2 Analysis of macrocrack propagation

A material that will be used as a reference for further analyses is specified by the following parameters: E=22 GPa, ν=0.2, σ_{fc}=2.4 MPa, σ_{mb}=2.6 MPa, ε_{mb}^{c}=0.001 and δ_0=1.27 mm. These parameters are realistic for a cement paste/polymeric fibers composite, even though the ductility (ε_{mb}^{c} and δ_0) may be on the lower end of an achievable range (Li, 1997).

Fig. 4 shows the resistance curve computed for this material. Composite fracture energy G_c is calculated using Eqn. 4 directly from the applied stress intensity K when crack growth occurs. The figure also shows component G_b, calculated as J integral along the localized bridging zone. As derived by Rice (1968), G_b can be expressed as:

$$G_b = \int_0^{\delta} t_n(\delta_n)\, d\delta_n, \tag{11}$$

where δ is the normal displacement jump at the end of the localized bridging zone. When macrocrack growth occurs, $\delta=\delta_0$ and Eqn. 11 yields (for a linear tension softening relationship):

$$G_b = \sigma_{mb}\delta_0/2 \tag{12}$$

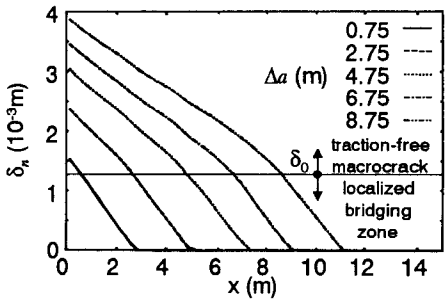

Fig. 5 Localized bridging zone and traction-free macrocrack profiles at different amounts of macrocrack extension

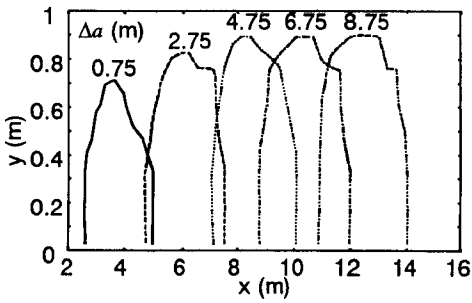

Fig. 6 Zones of 'active' multiple cracking at different amounts of macrocrack extension

Obviously, G_b is independent of the macrocrack extension Δa. Note that off-crack-plane fracture energy G_m is the difference between G_c and G_b.

Fig. 4 reveals that at the macrocrack growth initiation, both components of fracture energy G_m and G_b have non-zero values. This results from the fact that energy is dissipated through both distributed multiple cracking and formation of localized bridging zone prior to the traction-free macrocrack growth. As the macrocrack extends, the total fracture energy increases, due to the increase in component G_m, until it reaches almost constant value at Δa equal to about 5m. This behavior can be explained analyzing Fig. 5 and Fig. 6. Fig. 5 shows that the localized bridging zone profile and length are almost constant ever since the macrocrack starts to grow. On the contrary, the size and shape of an 'active' multiple cracking zone changes until the steady state is reached, as it is evident in Fig. 6. Here by 'active' zone we understand a region, in which energy dissipation associated with multiple cracking takes place, or in other words, yield condition of Eqn. 7 is satisfied.

Fig. 4 also displays values of J integral calculated using Eqn. 1 on a contour entirely enclosing the nonlinear zone. A good agreement with energy release rate G is observed, proving that small-scale yielding has been achieved. The difference between J and G at large Δa can be explained by accumulated error of the incremental finite element solution.

4.3 Parametric study

In order to identify uniaxial parameters that have a dominant influence on the composite fracture energy a parametric study was carried out. Individual effect of each of the following parameters was investigated: first crack strength σ_{fc} [Case a], stress increase capacity after first crack (σ_{mb}-σ_{fc})

[Case b], strain capacity ε_{mb}^{c} with hardening slope $(\sigma_{mb}-\sigma_{fc})/\varepsilon_{mb}^{c}$ constant [Case c], ε_{mb}^{c} with $(\sigma_{mb}-\sigma_{fc})$ constant [Case d], and slope of tension softening relation s [Case e]. An FEM analysis similar to that discussed in Section 4.2 was carried out for at least three different values of each of the varied parameters, while keeping the remaining parameters constant and equal to those given in Section 4.2. Each computation was continued with increasing Δa until the fracture energy became invariant, or almost invariant, of Δa, providing both the composite fracture energy at macrocrack growth initiation and that in the steady state. Results of these analyses are presented in Fig. 7. The figure contains graphs of bridging fracture energy G_b, off-crack-plane fracture energy G_m at macrocrack growth initiation, and the steady-state value of G_m plotted against each of the varied parameters. The fracture energies are normalized by the bridging fracture energy of the reference composite from Section 4.2, which is 1.651 kJ/m^2. Each varied parameter is normalized with respect to its reference value given to it in Section 4.2.

As the dependence of the bridging fracture energy on the uniaxial parameters is clear from Eqn. 12, we concentrate our attention on the off-crack-plane component G_m.

As seen in Fig. 7, the value of G_m at initiation of the macrocrack growth appears to increase almost linearly with any of the studied parameters, except for the slope of tension softening relationship s [Case e]. In the latter case, increasing s causes reduction in G_m.

Analyzing Fig. 7, it can be noticed that increasing the first crack strength [Case a] has almost no effect on G_m in the steady state; actually, G_m slightly decreases with increasing σ_{fc}. The off-crack-plane fracture energy exhibits initially almost linear dependence on post-crack stress increase capacity $(\sigma_{mb}-\sigma_{fc})$ [Case b]. However, at higher values of $(\sigma_{mb}-\sigma_{fc})$, the relationship seems to flatten out. It is possible, though, that for the last point of the curve in Fig. 7.b), a steady state was not yet reached. The effect of parameter ε_{mb}^{c} when $(\sigma_{mb}-\sigma_{fc})$ is constant [Case d] also appears to be linear. Analyzing Fig. 7c), it is becomes clear that the most effective way to improve the steady-state value of G_m is to increase the strain capacity, while keeping the hardening slope $(\sigma_{mb}-\sigma_{fc})/\varepsilon_{mb}^{c}$ constant [Case c]. In this case, the growth of G_m appears to be almost quadratic. Note that to keep $(\sigma_{mb}-\sigma_{fc})/\varepsilon_{mb}^{c}$ constant, both ε_{mb}^{c} and $(\sigma_{mb}-\sigma_{fc})$ must increase proportionally. Thus, we can conclude that the effects of ε_{mb}^{c} and $(\sigma_{mb}-\sigma_{fc})$ multiply. Finally, Fig. 7e) shows that higher value of the tension-softening slope, which corresponds to a higher post-peak brittleness, results in decrease of G_m [Case e].

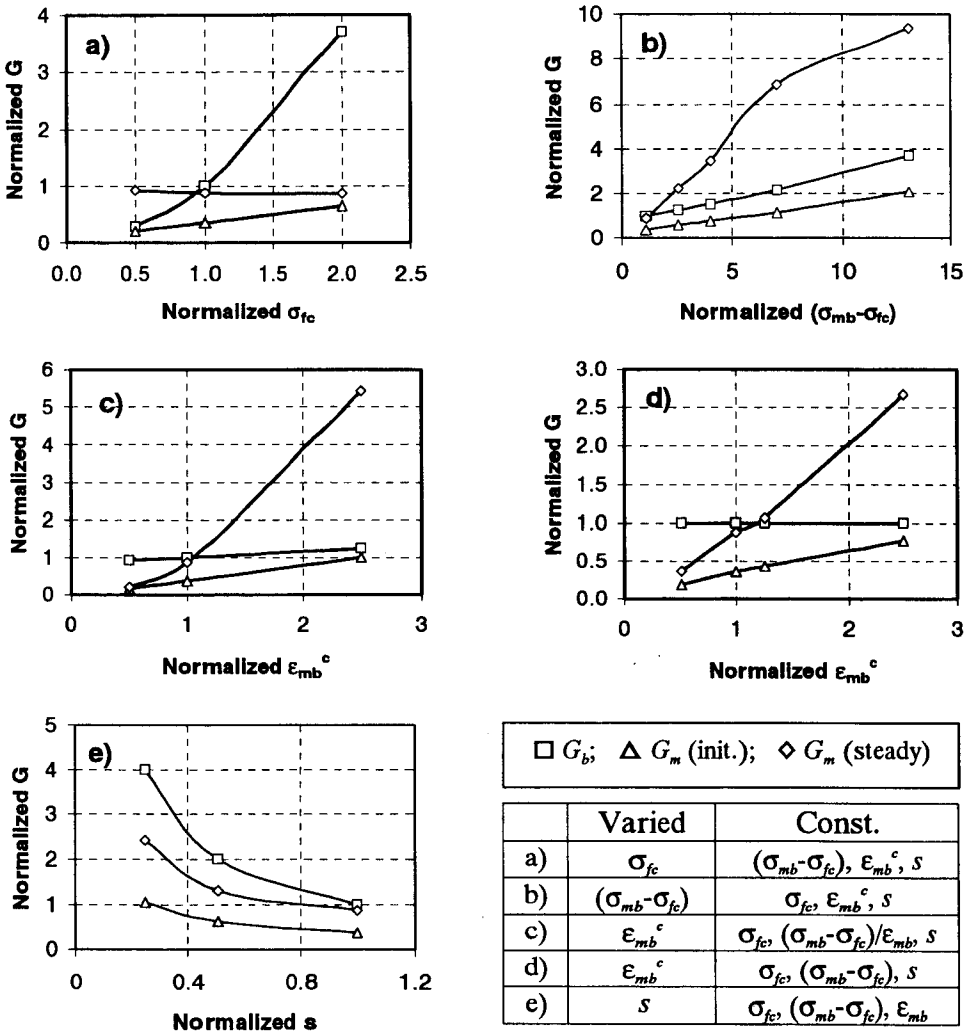

	Varied	Const.
a)	σ_{fc}	$(\sigma_{mb}-\sigma_{fc})$, ε_{mb}^{c}, s
b)	$(\sigma_{mb}-\sigma_{fc})$	σ_{fc}, ε_{mb}^{c}, s
c)	ε_{mb}^{c}	σ_{fc}, $(\sigma_{mb}-\sigma_{fc})/\varepsilon_{mb}$, s
d)	ε_{mb}^{c}	σ_{fc}, $(\sigma_{mb}-\sigma_{fc})$, s
e)	s	σ_{fc}, $(\sigma_{mb}-\sigma_{fc})$, ε_{mb}

Fig. 7 Results of parametric study

5 Final remarks

Attention has been paid mainly to the off-crack-plane fracture energy, as the dissipation mechanism that it associated with (distributed fine cracking) may be more desirable than the localized process that gives rise to the bridging fracture energy. However, it should not be forgotten that the bridging fracture energy may also significantly contribute to the composite fracture energy.

Finally, the applicability of the presented results should be discussed. The present analyses have been carried out under small-scale yielding conditions. In such a case, the nonlinear process zone where energy dissipation takes place is not limited by the boundaries of the structure or specimen. It should be noticed that the nonlinear zone diameter was about 2 m for the reference composite in Section 4.2. Such a large zone may not be achievable in real applications. Thus, the composite fracture energy actually observed in finite size structures may be much lower than the results presented in this paper. However, these results are intended as guidance for a design of pseudo strain-hardening cementitious composites, which would have improved resistance against crack growth. For this purpose, the present work should prove itself useful.

6 Acknowledgement

The authors are thankful to Prof. Hideyuki Horii for his contribution and helpful discussions related to this work.

7 References

Broek, D. (1991) **Elementary Engineering Fracture Mechanics.** Kluwer Academic Publishers, The Hague.

Hutchinson, J. W. (1968) Singular Behaviour at the End of a Tensile Crack in a Hardening Material. **Journal of the Mechanics and Physics of Solids**, 16, 13-31.

Kabele, P. (1995) **Doctoral Thesis.** The University of Tokyo, Tokyo.

Kabele, P. and Horii, H (1997) Analytical Model for Fracture Behavior of Pseudo Strain-hardening Cementitious Composites. **Concrete Library of JSCE**, 29, 105-120.

Li, V. C. and Hashida, T. (1992) Ductile Fracture in Cementitious Materials?, in **Fracture Mechanics of Concrete Structures** (ed. Z. P. Bažant), Elsevier Applied Science, London, New York, 526-535.

Li, V.C. (1997) Engineered Cementitious Composites - Tailored Composites Through Micromechanical Modeling, to appear in **Fiber Reinforced Concrete: Present and the Future** (eds. N. Banthia, A. Bentur, and A. Mufti), Canadian Society of Civil Engineers.

Rice, J. R. (1968) A Path Independent Integral and the Approximate Analysis of Strain Concentration by Notches and Cracks. **Journal of Applied Mechanics Transactions of the ASME**, 379-386.